

<https://doi.org/10.1038/s44304-024-00031-w>

Compound dry-hot-fire events connecting Central and Southeastern South America: an unapparent and deadly ripple effect

Check for updates

Djacinto Monteiro dos Santos¹✉, Aline M. de Oliveira¹, Ediclê S. F. Duarte^{2,3}, Julia A. Rodrigues¹, Lucas S. Menezes¹, Ronaldo Albuquerque¹, Fabio de O. Roque^{4,5}, Leonardo F. Peres¹, Judith J. Hoelzemann² & Renata Libonati^{1,6}✉

South America has experienced severe compound drought-heatwaves (CDHW), exacerbating fires. Recently, the unprecedented Pantanal 2020 fire season (P20F), burning a third of the biome, resulted in well-reported local impacts on the ecosystem, economy, and health. Nevertheless, the long-range ripple effects of this event remain unknown. We investigated the P20F-related cascading hazards, integrating models, observational and satellite-based data. P20F-related smoke elevated PM_{2.5} levels in the SA's most populated area, exceeding WHO guidelines by up to 600%. Smoke-induced air pollution episodes coincided with widespread heatwaves, amplifying health risks. The mortality burden attributable to this multi-hazard short-term (14 days) exposure was estimated to be 2150 premature deaths (21% increase above expected levels). Our findings highlight that the impacts of CDHW-fires in SA are beyond the local level, implying growing challenges for risk management and public health and the need for governance based on telecoupled flows, linking different systems over multiple scales.

Extreme weather events have become more frequent, longer, and intense due to anthropogenic global warming¹. These events can occur independently from each other but also simultaneously (compound events) or sequentially (cascading hazards)² amplifying their overall effects^{3,4}. Drought conditions, for example, can exacerbate heatwaves, increasing fire risk⁵. Vegetation fires, in turn, can contribute notably to local, regional^{6–8}, and global air pollution. While single impacts of isolated weather-driven natural extreme events are well understood, a significant gap remains in our knowledge of how these impacts accumulate when combined so that considering such events independently can lead to misestimating the magnitude, intensity, and duration of the involved processes and their actual risk⁹. Therefore, understanding the complex relationships and feedback mechanisms between extreme events is crucial for risk assessment, which requires integrated approaches considering the interconnected nature of these hazards¹⁰.

In recent years, substantial efforts have been made towards understanding compound events and cascading hazards caused by the combination of several drivers. During Australia's 2019/2020 fire season, for

example, moderate rain and floods following extreme drought and subsequent wildfires had their impacts amplified due to increased surface runoff, leading to reductions in water quality and rising ash and soil erosion in the country's east coast⁹. In the United States, the record-breaking 2021 heatwave was associated with a preexisting drought that exacerbated the escalation of temperatures¹¹. In western Russia, land-atmosphere interactions intensified drought conditions, promoting the advection of warm and dry air, developing the heatwave downwind, and resulting in cascading impacts in 2010 due to a coupled lack of rainfall and enhanced evaporative demand¹².

Climate-related extreme hazards pose severe threats to natural and human systems, including infrastructure, livelihoods, ecosystems, and human health, thereby contributing to societal and environmental risks¹³. For instance, in Moscow, over 2000 excess deaths were attributed to the interaction between high temperatures and air pollution from wildfires during the 2010 Russian heatwave¹⁴. In Brazil, studies have shown a positive association between exposure to drought¹⁵ and heat¹⁶ with increased mortality, particularly affecting females, children, and older adults. Regarding

¹Departamento de Meteorologia, Universidade Federal do Rio de Janeiro, Rio de Janeiro, Brazil. ²Department of Atmospheric and Climate Sciences, Graduate Program in Climate Sciences, Federal University of Rio Grande do Norte, Natal, Brazil. ³University of Évora - Institute of Earth Sciences, Évora, Portugal.

⁴Universidade Federal de Mato Grosso do Sul, Campo Grande, Brazil. ⁵Center for Tropical Environmental and Sustainability Science (TESS) and College of Science and Engineering, James Cook University, Cairns, QLD, Australia. ⁶Instituto Dom Luiz (IDL), Faculdade de Ciências, Universidade de Lisboa, Lisboa, Portugal.

✉e-mail: santos.djacinto@gmail.com; renata.libonati@igeo.ufrj.br

extreme heat, 37.0% of warm-season heat-related deaths globally can be attributed to current human-induced climate change, reaching 60% in Brazil¹⁷. In the Amazon region, drought and vegetation fires have increased respiratory disease hospitalizations, with compounded effects significantly impacting older adults and children¹⁸. Additionally, a projected increase in warm-season mortality from the 2000s to the 2090s is expected across various climate zones under different climate change scenarios, shifting the mortality peak from cold to warm seasons in arid, temperate, and continental zones¹⁹.

Although the analysis of compound events and cascading hazards is poorly documented in South America (SA)^{20,21}, recent global studies point out the continent as a current and future hotspot for these events^{22,23}. A recent showcase was the severe 2019–2022 outstanding drought over central-east SA coincident with several heatwaves^{24,25}. Notably, in 2020, compound drought and heatwave (CDHW) conditions triggered the worst fire season in the last two decades over the Pantanal (Fig. 1), the largest contiguous wetland in the world²¹. Land-atmosphere feedback contributed decisively to the unprecedented wildfires registered in the region, with approximately 70% of the burned area that year attributed to CDHW events²⁶. The Pantanal 2020 fire season (P20F) accounted for more than 3.9 million ha burned, an area four times larger than the long-term average^{27,28}, with several impacts on the ecosystem^{29,30}, hydrological cycle³¹, the economy³², and on the COVID19-associated hospitalizations^{33,34}. Despite the notable advance in understanding the local effects of the P20F-related CDHW-fires, multi-hazard evaluations still need to be addressed; therefore, the widespread knock-on effects still need to be explored.

Here, we investigated the cascading chain of hazards associated with the CDHW-fire events during the P20F beyond the local perspective by linking the smoke transport, the worsening air quality, and the health impacts in the São Paulo state (SPS) in southeastern Brazil (Fig. 1), which includes the Metropolitan Area of São Paulo (MASP), the largest SA megacity located approximately 1.500 km from Pantanal with over 21 million inhabitants (according to Brazilian 2022 census). Moreover, local weather and environmental conditions over the SPS were investigated as interconnected processes that could amplify/reduce such impacts. We combine different data sets, satellite-derived fire products, and atmospheric models, providing multiple lines of evidence of the long-range cascading impacts of the CDHW-fire events from the P20F on the southeast region of SA.

Results

Cascade chain: a storyline for the unprecedented Pantanal Fires in 2020

The year 2020 was the driest in the Pantanal since at least 1980^{35,36}, which took place under an outstanding drought that lasted from 2019 to 2022²⁵ depicted by the most significant negative peaks in the monthly SPEI-6 time-series (Fig. S1). These prolonged drought conditions resulted from changes in the Walker and Hadley Cells' circulation and the establishment of a Rossby wave extending from the west South Pacific towards South America²⁵, associated with the rare consecutive three La Niña events^{37,38}. In the months preceding the fire season, large precipitation deficits were observed, close to zero for most days (Fig. S2a), leading to record-breaking (the lowest value since 1951) negative soil moisture anomalies²⁶. Notably,

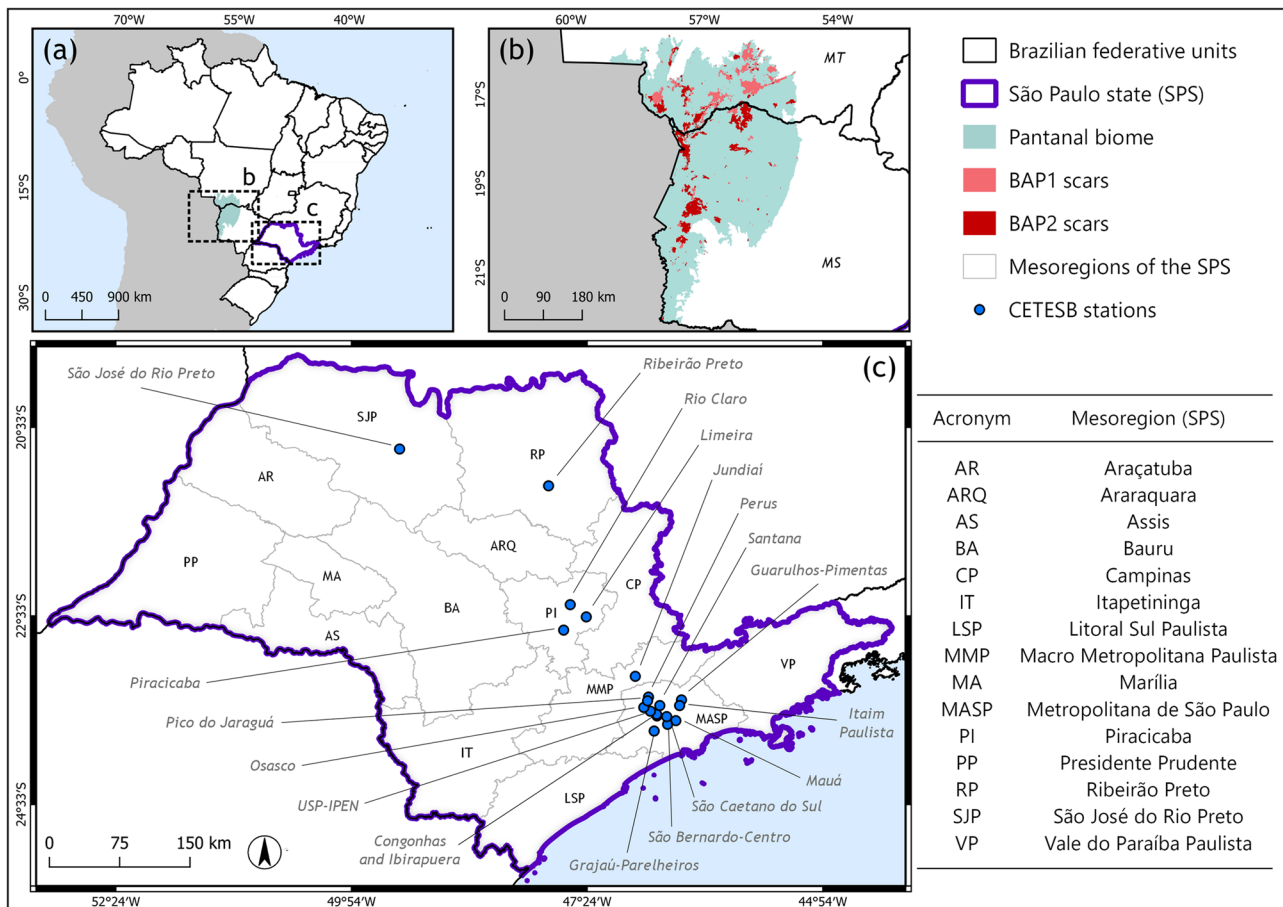


Fig. 1 | Map of the study area. a Geographical location of São Paulo state (SPS) and Brazilian Pantanal, (b) scars from the first and second peaks of burned area in 2020 over the Pantanal (BAP1 and BAP2), and (c) the location of CETESB monitoring

stations. The SPS is divided into 15 mesoregions labeled according to their acronyms. Map created using the Free and Open Source QGIS.

the 2020 drought was simultaneously marked by unprecedented extreme hot conditions, which favored land-atmosphere feedback, amplifying fire episodes^{21,26,39,40}. Three consecutive heatwaves occurred between August and October, with temperature anomalies reaching 6 °C (Fig. S2b). According to Libonati et al.²¹, two distinct mechanisms have fueled fire occurrence in a cascading effect during the short span of these CDHW events. First, unprecedented long-term deficits in precipitation and significant evaporation rates dry out the soil and vegetation, reducing flood pulse and fueling fires. Second, increased sensible heat surface-atmosphere flux and soil desiccation establish a water-limited regime, boosting the concurrence of extreme heat and rising flammability thresholds²⁶. Although CDHW conditions last for only 37% of the fire season, they accounted for 71% of the burned area in the Brazilian Pantanal²¹.

Two significant peaks of BA were identified during the CDHW period (Fig. S2c). The first BA peak (hereafter BAP1) occurred between September 9th and 17th (9 days), accounting for 618.6 kha, and the second (hereafter BAP2) between September 25th and October 11th (17 days) and reaching 887.6 kha (Table 1). In this context of CDHW-fire conditions, the 2020 fire season was unprecedented, with monthly BA exceeding the historical average by up to 5 times (Fig. S2d). Notably, BAP1 and BAP2 presented a temporal match with intense heatwave periods (Fig. S2b) from 5 to 20 September and between 25 September and 15 October. Burned area during the BAP1 was concentrated in the Pantanal of the Mato Grosso state, while occurrences in BAP2 were concentrated in the west and central north of the biome (Fig. 1b). A brief description of BAP1 and BAP2 is presented in Table 1.

Large-scale cascading hazards: from local to long-range effects

We investigated the smoke transport from the CDHW-fire events during the P20F to the SPS through HYSPLIT trajectory simulations (Fig. 2) during the BAP1 and BAP2 periods. Overall, air mass trajectories from the Brazilian Pantanal were advected towards the south of the country during the analyzed periods. However, three noteworthy episodes of smoke transport were identified in the southeastern direction reaching SPS. The first episode (T1) occurred at the end of BAP1 (September 17), as confirmed by both forward (Fig. 2a) and backward (Fig. 2d) trajectories starting in the Pantanal and ending in the MASP. In particular, backward trajectories above the atmospheric boundary layer indicate a long-range transport pattern. The second episode (T2) occurred during the BAP2 (September 27), as observed for forward (Fig. 2b) and backward (Fig. 2e) trajectories. The third episode (T3),

also during BAP2, occurred on October 7, reaching the SPS on October 9 (Fig. 2c, f). A brief description of T1, T2, and T3 is presented in Table 1.

During T1, T2, and T2 episodes, EURAD-IM model simulations (Fig. 3) showed significant contributions from the Pantanal emissions to the PM_{2.5} levels in large areas of the SPS both at the surface level and at 850 hPa. The role of the SA Low-Level Jet (SALLJ)⁴¹ in transporting the smoke plumes from the Pantanal is evident from the wind patterns at 850 hPa (Fig. 3d–f). EURAD-IM model quality indicators are shown in Tables S1 and S2.

PM_{2.5} simulations showed high concentrations in regions with extensive fire activity during T1, T2, and T3 episodes (Figs. S3, S4, and S5), including the Brazilian Pantanal, Bolivia, northern Argentina, and SPS. Particularly at the SPS, it can be attributed to the high number of active fires in the state (Fig. S6) in August, September, and October, reaching 5591, 14,567, and 6879 fires, respectively (compared to <500 fire counts in the other 2020 months). Relative to the monthly climatology, the total fire count in September and October 2020 was approximately twice the average for these months from 2012 to 2023 (excluding 2020) (Fig. S6b). In particular, September 13th and 14th were the top fire days, with 2030 and 1335 fires, respectively (Fig. S6a). However, a sharp decrease in the fire counts was observed in the following days, so the contribution of local fires during the T1 is expected to be small. Despite being lower, peaks of local fire activity were also observed near T2 (1295 on October 1st) and T3 (1280 on October 7th). Therefore, although the significant influence of smoke from CDHW-fire events during the P20F on PM_{2.5} levels over SPS during transport episodes, the contribution of the local fire emissions cannot be neglected.

In 2020, the highest PM_{2.5} concentrations in the SPS were observed during the dry months (May to October), surpassing both the Brazilian 24-hour air quality guidelines established by the Conselho Nacional do Meio Ambiente (CONAMA) (25 µg/m³) and the World Health Organisation (WHO) standards (15 µg/m³ in 24 h), on most days (Fig. 4). In particular, notable PM_{2.5} peaks concurrent with the T1, T2, and T3 were observed in most state mesoregions. The first PM_{2.5} peak (PMP1) occurred on September 18th–19th, encompassing all mesoregions. The sharp rise in concentrations simultaneously with the T1 indicates a substantial contribution of smoke transport from the Brazilian Pantanal during the BAP1 period to the PMP1, corroborating the results of the EURAD-model simulations. In particular, daily averages reached 70 µg/m³ in the MASP (in São Caetano do Sul station) and 115 µg/m³ in Ribeirão Preto. Despite the high PM_{2.5} levels, PMP1 was a short-term peak, with low concentrations (<10 µg/m³) from September 20th.

The second PM_{2.5} peak (PMP2) extended from September 29th to October 3rd, with daily averages above 30 µg/m³ for most CETESB stations during the five days. Exceptionally, in the MASP, the PMP2 was later and shorter, from September 30th to October 2nd. In the MASP, the concentrations reached a maximum on October 2nd, ranging between 33 µg/m³ (Pico do Jaraguá station) and 50 µg/m³ (Osasco station), while for the other mesoregions, the peak occurred on October 3rd, with daily averages in the 40 to 50 µg/m³ range. The PMP2 period fits with T2 dates, indicating the contribution of smoke transported from P20F during the BAP2 to the high-PM_{2.5} episode. Overall, concentrations decreased on October 4th, except for Ribeirão Preto and São José do Rio Preto. Particularly in the MASP, were below 10 µg/m³ PM_{2.5} levels after PMP2.

The third PM_{2.5} peak (PMP3) covered the period between October 5th and 9th, with daily averages above 30 µg/m³ across the SPS, reaching 85 µg/m³ in São José do Rio Preto on October 9th. Although the maximum PM_{2.5} levels during the PMP3 fits the T3 dates in most mesoregions, suggesting the contribution of smoke transported from P20F, this air pollution peak appears to be associated with a combination of factors. First, the high PM_{2.5} levels over the SPS occurred a few days after the PMP2 and, therefore, can be related to the persistence of the smoke in the atmosphere. Moreover, it can also be attributed to local fire emissions since a high number of active fires was observed on October 7th in SPS (Fig. S6). In São José do Rio Preto and Ribeirão Preto, the PM_{2.5} levels remained high between PMP2 and PMP3. Therefore, in these mesoregions, PMP2 and PMP3 can be interpreted as a single smoke-induced PM_{2.5} peak.

Table 1 | Summary of relevant information about the peaks of burned area in the Brazilian Pantanal, transport episodes, and smoke-induced PM_{2.5} peaks in the SPS

Peaks of Burned Area	Period	Burned Area [kha]	Simultaneous CDHW period
BAP1	9 Sep–17 Sep	618.6	Sep 5–Sep 20
BAP2	25 Sep–11 Oct	887.6	25 Sept–15 Oct
Transport Episodes	Starting dates (from Brazilian Pantanal)	Arrival dates (in the SPS)	
T1	17 and 18 Sep	18 and 19 Sep	
T2	26 and 27 Sep	28 and 29 Sep	
T3	7 Oct	9 Oct	
Smoke-induced PM _{2.5} Peaks	Period	Multi-site daily PM _{2.5}	
PMP ₁	Sep 18–19	17–112 µg/m ³	
PMP ₂	Sep 29–Oct 3	9–54 µg/m ³	
PMP ₃	Oct 5–Oct 9	11–85 µg/m ³	

The total burned area and simultaneous CDHW periods during the burned area periods are also shown. The PM_{2.5} daily averages during the smoke-induced PM_{2.5} peaks are presented as a multi-site concentration range.

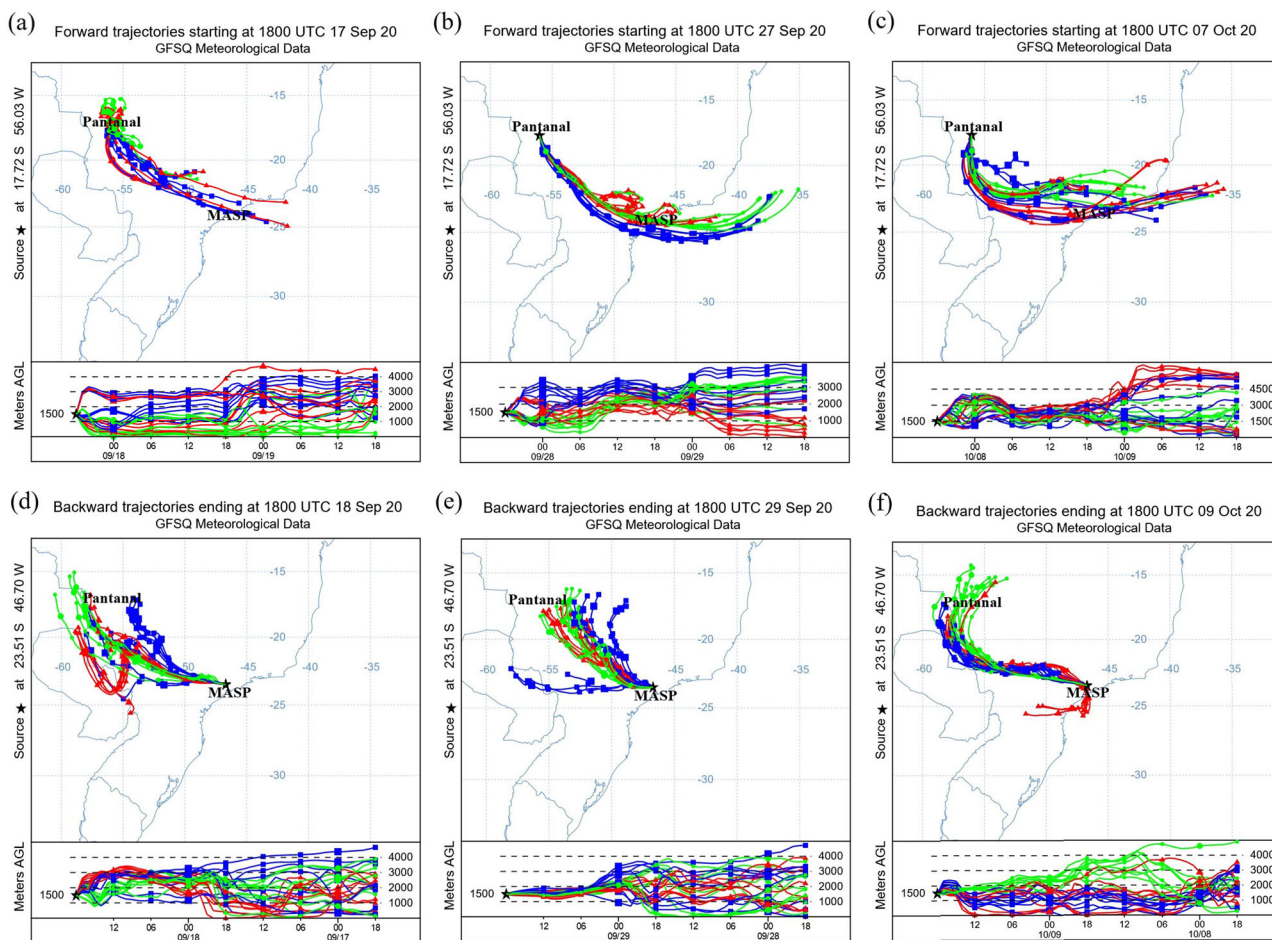


Fig. 2 | Airmass trajectories and long-range transport of P20F-related smoke. HYSPPLIT 48-h air-mass trajectories during the three episodes of transport of smoke from the Brazilian Pantanal to the SPS (T1, T2, and T3), including forward trajectories starting in the Pantanal at 1800 UTC on (a) September 17, (b) September 27, (c) October 7, and backward trajectories ending in the Metropolitan Area of São Paulo (MASP) at 1800 UTC on (d) September 18, (e) September 29, and (f) October 9, respectively.

Cascading risks: public health implications and multiple hazard synergy

The distribution of non-COVID-19 mortality in the SPS is presented in Fig. 5. A very different pattern was observed in 2020 (blue and red lines) compared to the previous ten years (black line). A substantial increase in daily non-COVID-19 deaths was observed from February to June 2020 (Fig. 5a), markedly in the first months of the pandemic, mainly due to an outbreak of respiratory-related deaths (Fig. S7). These findings are in close agreement with those observed in eight of the largest Brazilian urban centers, including São Paulo city¹². According to the authors, from February 23rd to August 8th, the excess mortality from respiratory system diseases was 312% in the cities analyzed. Although São Paulo had the lowest increasing rate among the cities included in the referred study (174%, while in Manaus, in the north of the country, this number reached 758%), this is equivalent to 7780 excess deaths from respiratory diseases in the period. The authors attributed the high number of excess respiratory deaths to the high underreporting of deaths from COVID-19 at the beginning of the pandemic. Despite these issues, from July onwards, the distribution of mortality in 2020 tends to be closer to the expected. This normalization can be explained by improving the diagnosis of COVID-19 deaths, reducing underreporting, and, therefore, reducing the overestimation of respiratory deaths.

A substantial rise in non-COVID-19 deaths was observed in the period from October 1st to October 14th, reaching 12,602 deaths across SPS. The period covers both PMP2 and PMP3. Compared to the expected mortality ratio, it represents 2150 (2095–2206) excess deaths in a 14-day window, with an observed-to-expected ratio of 1.21 (1.17–1.24). When looking at the

regional distribution of the excess deaths, however, we observed that the mortality effects were not homogeneous throughout the mesoregions (Fig. 5b). In the western SPS (closer to the Brazilian Pantanal) and more impacted by smoke-induced PM_{2.5} during PMP2 and PMP3, the mortality increase was higher (128.0% in Araçatuba, 112.4% in São José do Rio Preto, 78.4% in Marília). Conversely, in the eastern part of the SPS (mesoregions Itapetininga, Litoral Sul Paulista, Metropolitana de São Paulo, and Vale do Paraíba Paulista), mortality increase was not statistically significant (Table S4).

Comparing the P20F-related mortality burden with control cases (previous heatwaves and fire-count spike days that occurred in the SPS in September or October months) provides an assessment of the expected impact of such events if they occur alone (Fig. 5c). Considering fire-count spike days (state daily number of active fires higher than the 95th percentile between 2012 and 2019), the mortality increase over the state was below 5% (median), both on the fire day (D) and on subsequent days (D + 1, D + 2 or D + 3). For state-wide heatwave days (i.e., heatwaves that affected more than 90% of the SPS area and occurred between 2008 and 2019), the impact was estimated at 10% (median). Both estimations are significantly lower than the 21% mortality increase observed within the 14-day window of coexposure to extreme heat and P20F-related air pollution.

CDHW events exacerbated fire risk in the Pantanal, promoting two main periods of burned area peaks (BAP1 and BAP2). Three episodes of long-range smoke transport to the SPS (T1, T2, and T3) were identified during BAP1 and BAP2 periods. Accordingly, three PM_{2.5} peaks related to T1, T2, and T3 were observed throughout the state (PMP1, PMP2, and PMP3). Among these episodes, PMP2 and PMP3 were simultaneous to a

Increment of PM_{2.5} Concentration from the Pantanal Megafires - GFAS Fire emission over Pantanal

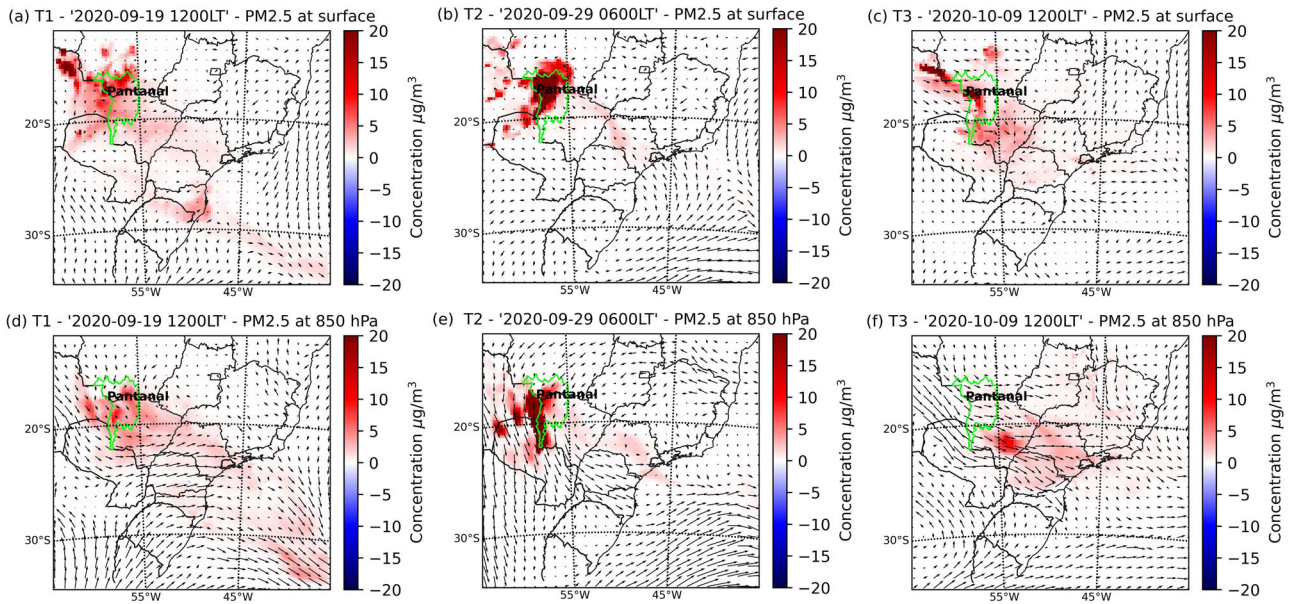


Fig. 3 | Contributions of the Pantanal fires to air pollution in the SPS. Increment from GFAS Pantanal in PM_{2.5} concentrations modeled with the EURAD-IM on September 19 (T1), September 29 (T2), and October 9 (T3) at surface level (a, b, and c, respectively) and 850hPa (d, e, and f, respectively).

Fig. 4 | Ground-level PM_{2.5} concentrations over the SPS in 2020. Daily PM_{2.5} mean concentration [$\mu\text{g}/\text{m}^3$] from CETESB monitoring stations in the mesoregions of São José do Rio Preto (SJP), Ribeirão Preto (RP), Piracicaba (PI), Macro Metropolitana Paulista (MMP) and Metropolitana de São Paulo (MASP). For the PI and MASP mesoregions, the multi-site mean and standard deviation are presented. The red dotted lines represent a threshold of 30 $\mu\text{g}/\text{m}^3$ (two times WHO air quality guidelines). The red bars represent the PMP1, PMP2, and PMP3 periods.

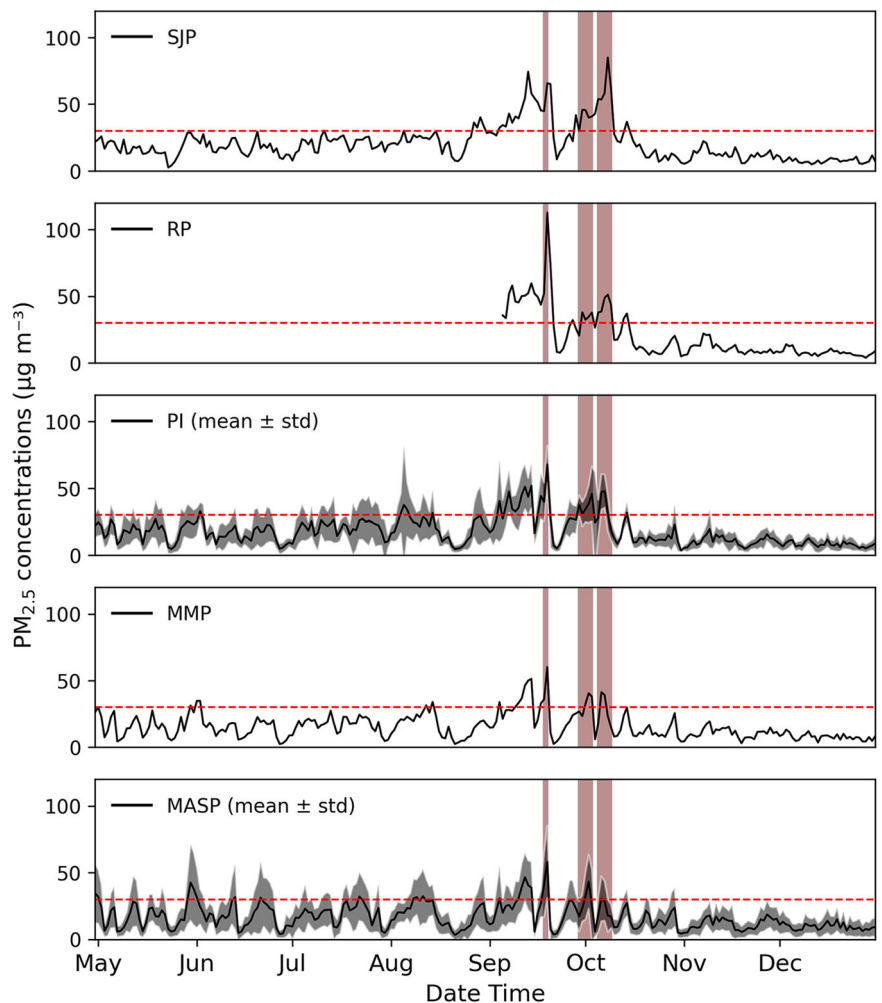
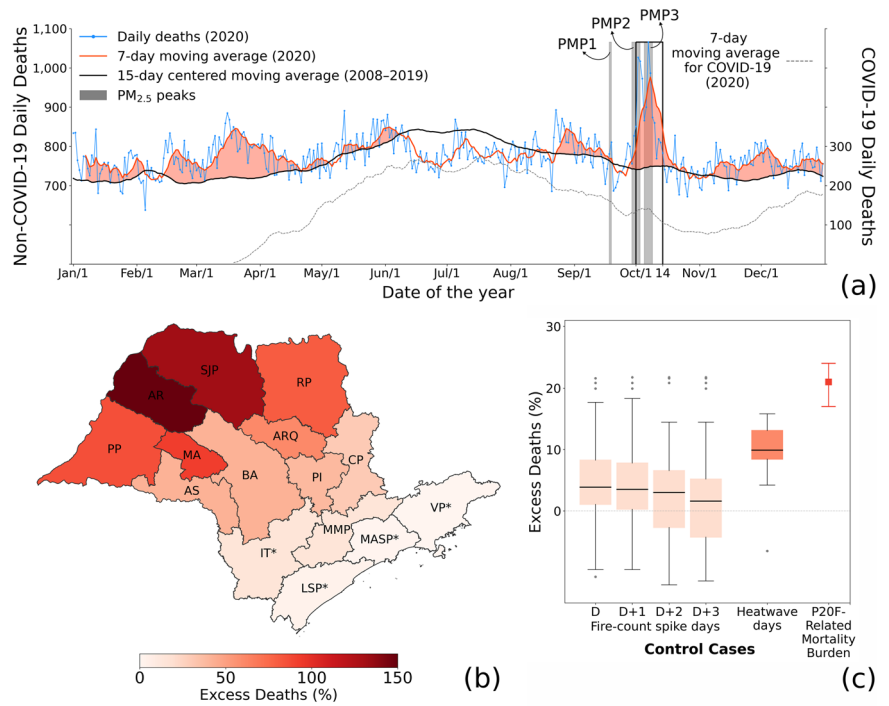


Fig. 5 | Daily mortality over the SPS. **a** Daily non-COVID deaths over the SPS throughout 2020 (blue), including the corresponding 7-day moving average (red). The black line shows the expected mortality (15-day centered moving average considering the mean values of daily deaths for the 2008–2019 period). The dark gray dotted line on the secondary y-axis represents COVID-19 deaths. The gray bars represent the smoke-induced PM_{2.5} peaks (PMP1, PMP2 and PMP3). **b** Excess mortality across SPS mesoregions from October 1st to October 14th. **c** Excess deaths observed during control cases that occurred in the SPS, including fire-count spike days alone from 2012 to 2019 (light red boxplots) and heatwave days alone from 2008 to 2019 (orange boxplot). The red error bar shows the P20F-related mortality burden estimated in the present study.



large number of non-COVID-19 excess deaths in the SPS, especially in the northwestern SPS, closer to the Brazilian Pantanal, where large increments of PM_{2.5} were attributed to the P20F through EURAD simulations. In this context, quantitatively determining the isolated effect of high PM_{2.5} levels on mortality rates is quite complex. Some hypotheses can be formulated from a more in-depth analysis of meteorological conditions over the SPS.

Overall, we observed an inverse correlation between daily precipitation and the duration of the PM_{2.5} peaks (Fig. 6). The rainfall is expected to play a significant role in reducing PM_{2.5} levels via particle wet deposition processes. In particular, the PMP1 was a short-duration peak (2 days). The sharp decrease in concentrations can be attributed to precipitation in the days following the peak (3, 6, and 10 mm on September 20th, 21st, and 22nd). Conversely, the PMP2 occurred in the absence of precipitation (September 29th to October 3rd), which may have contributed to the extensive time interval with high PM_{2.5} concentrations during the PMP2. Regarding PMP3, a behavior similar to PMP1 was observed, with a sharp decrease in concentrations and an increase in rainfall (2 and 8 mm on October 8th and 9th).

The distribution of daily mean temperatures (DMT) in the SPS also provides insights into the PM_{2.5} dynamics during the smoke-induced air pollution episodes. In particular, the days after PMP1 (20–21 September) are marked by a significant drop in DMT (Fig. 6a). Conversely, the PMP2 and PMP3 episodes occur in a period characterized by atypically high temperatures over the state. Compared to the respective climatological averages (1981–2010), all mesoregions presented positive temperature anomalies that began on September 24th, persisting for up to 16 days (encompassing PMP2 and PMP3). Over the state, the maximum anomalies in this period ranged from 4 to 12 °C, reaching higher values in the central part of the SPS (Fig. 6b). All mesoregions were under an HW regime (Fig. 6), from September 28th, with a duration varying from 7 days (in the mesoregions of Itapetininga, Litoral Sul Paulista, Macro Metropolitana Paulista, and Metropolitana de São Paulo) and 12 days (in the mesoregions Araçatuba, Araraquara, Presidente Prudente, Marília, Assis, Ribeirão Preto and São José do Rio Preto), with a significant coastal-to-inland gradient (lower duration in mesoregions closer to the ocean).

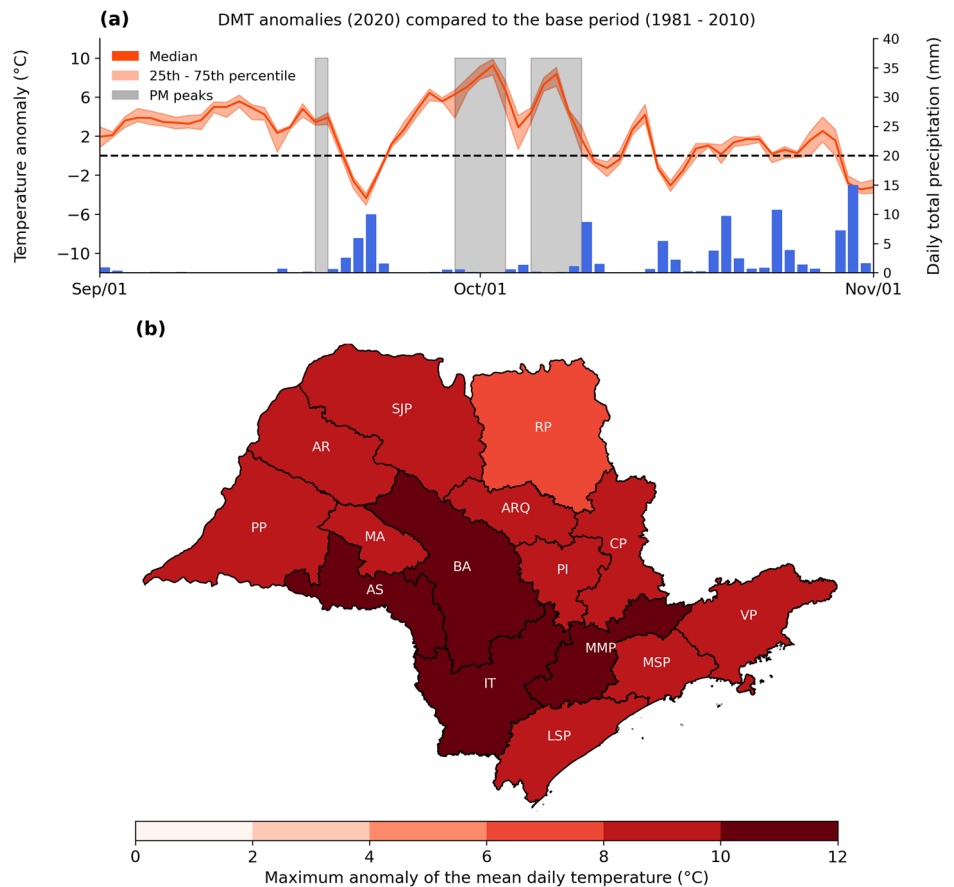
Notably, synoptic atmospheric blocking conditions were observed in the central region of Brazil during the 2020 dry season, which were

widespread and affected southeastern Brazil, including the SPS^{24,25}. The observed blocking patterns exhibited a large anticyclonic anomaly responsible for air subsidence, persistent clear sky conditions, low humidity levels, and episodes of absence of precipitation²⁶. These specific weather conditions and the occurrence of extreme temperatures in the SPS between September 28th and October 9th may have been responsible for the worsening of the air pollution condition, maintaining high pollution levels between the PMP2 and PMP3 periods and amplifying the effect caused by the transport of smoke during T2 and T3. Conversely, the rapid improvement in air quality after PMP1 may be linked to a sudden decay of the blocking pattern followed by a return to transient waves and precipitation. Moreover, the co-occurrence of extremely hot weather and air pollution episodes is expected to amplify the impact on health beyond the sum of their effects individually^{43,44}.

Discussion

CDHW events triggered uncontrolled fires during the 2020 dry season. Significant deficits in precipitation and large land evaporation rates pre-fire season combined with soil moisture-temperature feedbacks have boosted the occurrence of extreme heat and the unprecedented P20F²¹. Natural and anthropogenic mechanisms coupling has been responsible for cascading effects elsewhere. In Portugal, for example, the 2017 record-breaking burned area was attributed to the combination of prolonged drought, extensive vegetation hydric stress, the passage of a hurricane, and human actions (negligent ignitions)⁴⁵. The CDHW-fire events during the P20F were widespread, affecting environmental conservation areas, traditional communities, indigenous lands, and settlements⁴⁶. The impacts included 17 million killed vertebrates²⁹, decreasing post-fire vegetation productivity and increasing runoff³⁰, national economic losses of ~USD 3.6 billion⁴⁷, and health effects, increasing COVID-19 hospitalizations among older people³³. The wide range of local impacts reinforces the claims for developing integrated fire management (IFM) in the region^{21,26–28}, strengthening prevention actions⁴⁸. Despite recent advances in reducing burned areas, fire intensity, and associated emissions, IFM is still restricted to a few protected areas in Brazil^{49–51}. Thus, expanding IFM is necessary, besides strengthening environmental protection laws and sustainable land management policies countrywide.

Fig. 6 | Dry-season daily surface temperature anomalies and precipitation over the SPS. Daily mean temperature (DMT) anomalies in the state mesoregions and daily total precipitation as depicted by the (a) time series and (b) maximum DMT anomaly in each grid cell between September 27th and October 7th. Anomalies were computed as the difference between the mean daily temperature in 2020 and the base period (1981–2010) for each mesoregion. The PMP1, PMP2, and PMP3 periods are represented by the gray bars in (a). Median and IQ intervals were calculated considering the average temperatures from each mesoregion.



Going beyond the local level, CDHW-fire events in the Brazilian Pantanal resulted in significant long-range cascading effects. We identified three episodes of smoke transport to the SPS related to the CDHW-fire events during the P20F. The SALLJ was important in transporting smoke from the P20F to southeastern Brazil, similar to what was previously observed in central Brazil and the Amazon basin^{46,52}. However, a deep understanding of long-range transport mechanisms in SA is still crucial to better predict and manage risks in smoke-impacted regions. It is worth highlighting that IFM strategies are generally designed based on traditional place-based governance (i.e., focusing on governance or management of individual places), such as parks, communities, municipalities, and states. Nevertheless, as our results suggest, such strategies and policies need to be improved by adopting a telecoupled governance perspective⁵³, which opens a new perspective of linkages between systems over multiple scales, across distance, and through time in the policy, human health, education, communication, economic, social, and management strategies, including flows between them⁵⁴. In particular, multisectoral and inter-ministerial strategies transcending state government spheres and international cooperation are needed.

Along with previous studies^{46,55}, our work highlights the role of the Pantanal fires in disrupting air quality across the country, as already recognized for fires in the Amazon and Cerrado^{56–58}. In particular, the smoke loading over the Brazilian Pantanal during the P20F was higher than over Amazonia⁴⁶. Within the framework of national and international political articulations, integrating fire policies and management, including environment, health, and infrastructure sectors, involving different regions and biomes, could help fire emission monitoring and create alert systems to help society avoid the consequences of fires in SA.

The chain of extreme events in the Pantanal combined with long-range transport directly impacted air quality in the SPS. Three smoke-induced PM_{2.5} peaks were identified over the SPS related to the CDHW-fire events

from the P20F, exceeding CONAMA and WHO standards. Overall, air pollution episodes in the SPS are attributed to low precipitation periods and poor vertical mixing and horizontal dispersion conditions⁴⁴. In the last decades, restrictive and regulatory measures reduced primary emissions from vehicular and industrial sources in the state, although secondary pollutants remain at high levels⁵⁹. In particular, vehicle-derived precursors may interact with compounds in the atmosphere, further elevating secondary pollutant concentrations⁶⁰. Local biomass burning emissions (such as waste burning and wood stoves⁶¹) and the transport of smoke from regional fires also appear as significant emission sources, worsening air quality in the region⁶². In 2014, biomass burning emissions contributed to 18.3% of PM_{2.5} during the winter, mostly related to the transport of particles from areas affected by sugarcane burning⁶³. The SPS is the leading sugarcane producer in Brazil, accounting for over 50% of the national production, with cultivation mainly located in the central, northwest, and western regions of the state⁶⁴. Despite the pre-harvesting biomass burning for sugarcane crops being responsible for high pollutant emissions in the region⁶⁵, the legislation established by the SPS law N°11.241/2002 to gradually end the burning practice by 2031 reflects the observed reduction in fire occurrences over the region, despite the increase of sugarcane cultivation area and production⁶⁶. Although emission control policies represent an essential step in improving air quality in urban and densely populated areas such as the SPS, our findings reinforce the importance of compound events in pollution levels at the regional scale, highlighting the interconnection between CDHW-fires and air quality in SA. Previous studies have reported similar effects of long-range smoke transport worsening regional air quality in Southeastern Asia⁶⁷, Australia⁶⁸, and the US⁶⁹. Therefore, our work underscores the need to align multisectoral and multicountry policies to promote air quality.

The coexposure to smoke-induced air pollution and extreme heat led to 2150 excess deaths throughout the SPS. The 14-day peak of non-COVID-19 deaths represented a 21% mortality increase statewide, being

more pronounced in mesoregions closer to the Brazilian Pantanal. Two $PM_{2.5}$ peaks (PMP2 and PMP3) occurred in the SPS during the period mentioned above, along with prolonged and state-wide heatwaves (7 to 12 days), with temperature anomalies ranging from 4 to 12 °C, potentially amplifying health effects throughout the SPS. In Brazil, short-term smoke exposure has been associated with significant mortality risks^{70,71}, increased hospital admissions⁷², and substantial economic losses⁷³. $PM_{2.5}$ exposure has also been linked to significant productivity-adjusted life years lost (5.11% for every 10 $\mu\text{g m}^{-3}$) and economic costs estimated at 268 billion dollars between 2000 and 2019⁷⁴. Regarding heat exposure, a recent study attributed approximately 50 thousand excess deaths to heatwaves in Brazilian urban areas between 2000 and 2018, 14,850 only in the MASP¹⁶. Besides health effects, significant socioeconomic impacts, such as supply-chain disruption effects, health costs, and labor productivity loss, are related to heat exposure, with most severe losses disproportionately concentrated in Central and Southern Africa, Southeast Asia, and Latin America⁷⁵.

Extreme heat conditions in the SPS likely amplified the health effects from smoke-induced air pollution transported from the Pantanal, in addition to the high number of active fires throughout the state, contributing to the worsening of air quality throughout the state. The simultaneous exposure to heat and air pollution has synergistic and cumulative effects on health since their impacts occur through similar pathophysiological pathways⁷⁶. High temperatures and air pollution can cause inflammatory reactions in the respiratory system, increasing respiratory deaths⁷⁶. In the cardiovascular system, short-term exposure to air pollution may disrupt compounds present in the blood. In contrast, heat exposure stresses thermoregulation ability and the immune system, increasing susceptibility to air pollution effects⁷⁷. Nonetheless, several limitations are still associated with quantifying multi-hazard interrelationships in impact, as the interaction between different hazards can result in a more significant effect than the sum of their individual effects⁷⁸. By comparing the 21% mortality burden associated with the P20F in the SPS with some single-event control cases (heatwaves and fire-count spike days alone), we assessed the exceptional nature of this burden and the potential individual effects of exposure to heat and air pollution from local fires across the state. During fire-count spike days, a mortality increase below 5% (median) was observed for events between 2012 and 2019.

Similarly, for state-wide heatwaves, the median excess mortality was 10% for events in the 2008–2019 period. Regarding heat exposure, the result was in close agreement with the observed by Monteiro dos Santos et al.¹⁶, despite the authors considering only the MASP region (around half of the SPS's population). This result suggests that neither extreme heat conditions in the SPS nor the high number of active fire outbreaks throughout the state can explain the 21% short-term (14-day) P20F-related mortality impact, reinforcing the substantial long-range health effects of CDHW-fire events in SA.

Although we considered only non-COVID-19 deaths, it is also worth mentioning that the pandemic context exerts additional strain on the healthcare system, potentially amplifying the mortality burden. Therefore, assessing health indicators in a pandemic is challenging, even for causes unrelated to the virus. In Europe, for example, the combined effect of COVID-19 and extreme temperatures resulted in an indirect amplification in heat-related mortality (>50% compared to previous years) as a consequence of the disruption of healthcare systems and the decrease in emergency room admissions due to fear of the population attending healthcare facilities⁷⁹. $PM_{2.5}$ exposure was identified as a risk factor, particularly in the Brazilian Pantanal, resulting in a 23% increase in hospitalizations by COVID-19 in the elderly³³.

Like previous catastrophic fire events, the 2020 Pantanal wildfires resulted not only from severe drought and extreme heat conditions but also from a complex interplay among extreme climate conditions, lack of management, and human-induced ignitions²⁷. It is worth mentioning that this event occurred during the COVID-19 pandemic, severely contributing to the lack of environmental law enforcement due to the COVID-19 lockdown²⁸. The pandemic hindered Pantanal firefighting, reducing the

number of firefighters and constraining their movements spatially and temporally. In particular, Indigenous firefighters, who represent a significant proportion of the workforce in the Pantanal, could only work in the Indigenous lands. Moreover, in the context of wide fire outbreaks in the Amazon, Atlantic Forest, and Cerrado biomes in 2020, several brigades had been working in other regions of Brazil under great pressure²⁸. Equally important, land cover changes are pointed out to have contributed to homogenizing the landscape, favoring the occurrence of those mega-fires³¹. Furthermore, human ignition sources, either by accident, negligence, or arson, are responsible for most wildfires⁸⁰.

The simultaneous occurrence of extreme events is projected to become more frequent under all future climate change scenarios, materializing as a chain of impacts that can trigger cascading hazards and systemic risks^{81–83}. Multiple scale interactions between co-occurring drivers and cascading hazards amplify the impacts compared to the individual occurrence of such hazards⁸². Therefore, addressing and preparing for the effects of climate change demand a thorough examination of the intricate interplays between heat, droughts, air pollution, and other extreme events, integrating it into risk assessments and strategic planning, supported by robust monitoring systems to enhance readiness for potential future cascading hazards¹³. Integrating observational, satellite-based, and reanalysis data, atmospheric dispersion models and death records, we provided multiple lines of evidence of a long-range cascade chain of hazards connecting central and south-eastern SA (Fig. 7). The simultaneous exposure to smoke-induced air pollution transported from the P20F and persistent state-wide heat conditions in the SPS, combined with high local fire incidence that further worsened air quality throughout the state, resulted in 2150 excess deaths. This 21% mortality increase attributable to a multi-hazard short-term exposure (14 days) was significantly higher than estimations for single-event control cases that occurred locally in previous years (heatwaves and fire-count spike days alone). Our results underscore the need for comprehensive risk management and public health strategies that address the long-range cascading impacts of compound drought-heatwave (CDHW)-fire events in SA. These impacts extend beyond the burned and immediate surrounding areas, affecting distant populations. This reinforces the necessity for countries to strengthen collaboration across global governance structures to develop successful adaptation strategies and provide scientific support for policy-making, addressing current scientific challenges and motivating future studies.

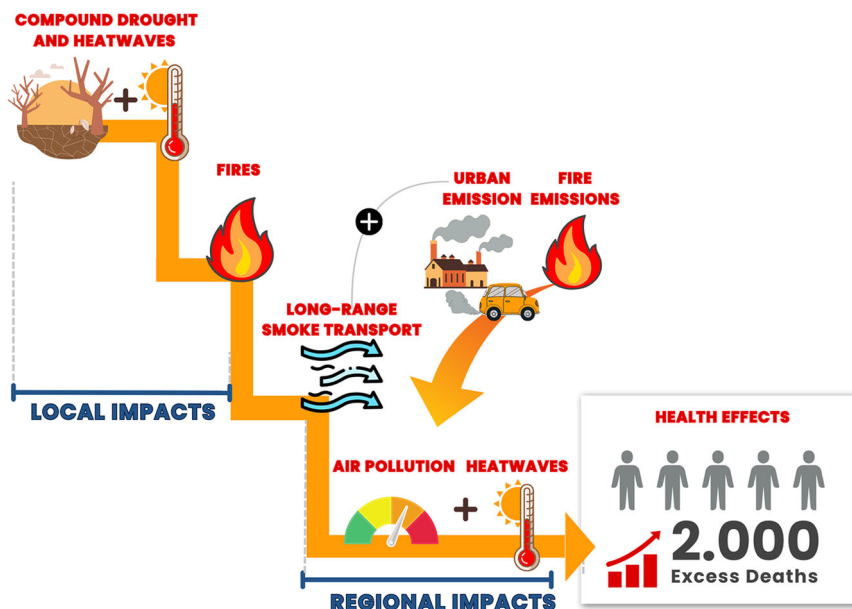
Methods

Study area

The Pantanal biome is the largest continuous wetland in the world⁸². The Brazilian Pantanal (Fig. 1), located in central-western Brazil (Fig. 1), covers an area of approximately 150,000 km², with a population of around 474,000 inhabitants (<https://ibge.gov.br/apps/biomas/>). The geomorphology and rainfall regime determine the flood pulse, beginning in the northern region during spring and moving toward the southern region⁸⁴. Fire in the Pantanal is mainly restricted to the dry season, from July to November⁸⁰, and occurs more frequently in the grasslands. Still, the 2020 fires have preferentially burned forests^{28,85}. Natural fires are rare in the Pantanal biome, accounting for less than 5% of the total fire scars⁸⁰. Thus, fire is generally associated with anthropogenic activities, particularly land use, land cover change, and management⁸⁶.

The São Paulo state (SPS), located in southeastern Brazil (Fig. 1), is the most populated in the country, with a population of 46.6 million inhabitants and an area of 248,219 km². The Metropolitan Area of São Paulo (MASP), comprising 39 municipalities, approximately 1,200 km from the Brazilian Pantanal, is the largest South American megacity with over 21 million inhabitants (<https://ibge.gov.br/cidades-e-estados.html>). The state is characterized by high pollution rates, especially in the MASP. However, successful public policies implemented in the region for controlling and monitoring the emissions from industries and a fleet of more than 8 million vehicles have led to a significant reduction in the emissions of primary atmospheric pollutants over the last decades⁵⁹. Additionally, local biomass

Fig. 7 | From local scale to long-range cascading effects: a schematic multi-hazard risk assessment framework connecting Central and Southeastern South America. Drought-heatwave coupling triggered fire risk and large burned areas in the Pantanal during the 2020 dry season. Long-range transport led to smoke-induced air pollution episodes in the São Paulo state, also influenced by local meteorological conditions and emission sources. Synergism and co-exposure to high levels of PM_{2.5} and extreme heat have resulted in a large burden of premature deaths. Map created using the Free and Open Source QGIS.



burning emissions, such as waste burning and wood stoves⁶¹, as well as the transport of smoke from forest fires upwind SPS, contribute significantly to worsening air quality throughout the state^{62,86}. The SPS is the leading sugarcane producer in Brazil, accounting for 54% of the national production (<https://conab.gov.br/info-agro/safras/cana>). Sugarcane cultivation is mainly located in the central, northwest, and west regions of the state⁶⁴, and the pre-harvesting biomass burning for sugarcane crops is responsible for high pollutant emissions in the area⁶⁵. In the MASP, Pereira et al.⁶³ estimated contributions of biomass burning for PM_{2.5} mass loadings ranging from 11.6% (annual average in 2014) to 18.3% (during the winter in 2014), mostly related to the long-range transport of particles from areas affected by sugarcane burning⁸⁷.

Satellite-derived burned area and fire data

The Burned Area (BA) over the Brazilian Pantanal was obtained from the first version of the *ALerta de Área queimada com Monitoramento Estimado por Satélite* - <https://alarmes.lasa.ufjf.br> - (ALARMES) satellite-derived annual dataset with 500 m spatial resolution for the main Brazilian biomes (Amazônia, Cerrado, and Pantanal). The algorithm combines daily images and active fires from the Visible Infrared Imaging Radiometer Suite (VIIRS) sensors and deep learning techniques to identify fire-affected areas⁸⁸. The product provides a layer with the approximate burn date and a confidence level layer representing the classification quality. Moreover, daily information on active fire counts over the SPS was obtained from NASA/NOAA's Visible Infrared Imaging Radiometer Suite (VIIRS) at 375 m (VNP141IMGTML)⁸⁹.

Weather data and heatwave definition

Data on air temperature at 2 m above the surface and total precipitation were gathered from the ECMWF reanalysis version 5 (ERA5), with a spatial resolution of 31 km and 1-h temporal resolution⁹⁰. The daily precipitation in 2020 over the entire SPS domain was computed from hourly data obtained from ERA5. The hourly temperature data were used to get each grid cell's daily mean temperature (DMT). Furthermore, DMT in each mesoregion was computed as the spatial average over the grid cells.

Following the methodology proposed by Nairn & Fawcett⁹¹, we used the Excess Heat Factor (EHF) to identify the occurrence of heatwaves in the mesoregions over the SPS. As a health-relevant heat index, the EHF has been widely used⁹², including recent studies in Brazil^{16,93}. The EHF is calculated as the product of two indices: (1) the significance index (EHI_{sig}), computed as the difference between the three-day-averaged DMT and the 95th percentile

of the DMT calculated across the 1981–2010 base period, and (2) acclimatization index (EHI_{accl}), which is calculated as the difference between the three-day-averaged DMT and the average DMT over the previous 30 days. Therefore, the EHF considers both the effect of short-term temperature anomalies and the human physical ability to adapt to them. If the EHF is positive, the three days are considered under heatwave conditions. More details about the methodology used here for heatwave identification can be found in ref. 16.

The drought severity was analyzed using the Standardized Precipitation Evapotranspiration Index at 6-month timescale (SPEI-6), derived from the ERA5 reanalysis product⁹⁴. The dataset was obtained directly through the SPEI Crop Drought Monitor (<https://global-drought-crops.csic.es/>), and drought severity was categorized according to the US Drought Monitor system (<https://droughtmonitor.unl.edu/About/AbouttheData/DroughtClassification.aspx>). The SPEI-6 provides insights into agricultural droughts related to shorter-length timescales⁹⁵ and has been preferred for assessing the dynamic water fluctuations in the Pantanal region. Its use is underscored by the established correlation between agricultural drought conditions and the incidence of wildfires⁹⁶.

Air quality data

Hourly PM_{2.5} [µg/m³] data were provided by the São Paulo State Environmental Company (CETESB, *Companhia Ambiental do Estado de São Paulo*, <https://cetesb.sp.gov.br/ar/qualar>) from 19 air quality monitoring stations across the SPS (Fig. 1) according to data availability. Data from CETESB monitoring stations have been largely used in air quality studies in the SPS⁵⁹. For most analysis, the CETESB stations were grouped according to the mesoregions where they are located, namely: RP (Ribeirão Preto), SJP (São José do Rio Preto), PI (Piracicaba, Limeira, and Rio Claro), MMP (Jundiaí), and MASP (Santana, Pico do Jaraguá, Perus, Itaim Paulista, Ibirapuera, Grajaú-Parelheiros, Congonhas, USP-IPEN, São Caetano do Sul, São Bernardo-Centro, Osasco, Mauá, and Guarulhos-Pimentas).

Mortality data and estimations of excess deaths

Daily mortality data from the Brazilian Health Informatics Department (DATASUS) were provided by the Data Science Platform applied to Health (PCDaS) of the Oswaldo Cruz Foundation (<https://pcdas.icict.fiocruz.br/>, accessed on February 06, 2022). Deaths related to external causes (accidents, suicides, and homicide) were not included in the analysis; moreover, confirmed deaths corresponding to code B34.2 (coronavirus infection disease)

were not considered. Total daily deaths from respiratory system diseases (cataloged in chapter X, according to the 10th revision of the International Statistical Classification of Diseases and Related Health Problems, ICD-10) for all municipalities within SPS were analyzed. Annual estimates of the population in the SPS provided by the Brazilian Institute of Geography and Statistics were used to normalize mortality data, reducing the effects of population growth on the estimations of the expected daily number of deaths. The analysis of mortality data was based on the observed-to-expected deaths (O/E) ratio¹⁶. This method allows for a percentage analysis, correlating the total daily deaths observed during 2020 with the daily deaths expected (15-day centered moving average of mortality between 2008 and 2019). Excess mortality was obtained by the difference between observed and expected daily deaths (O-E).

The observed-to-expected ratio was used to estimate excess deaths associated with long-range impacts of the CDHW–fire events from the P20F in the SPS. Moreover, some control cases that occurred in the SPS were compared with the P20F-related multi-hazard event. For that, the observed-to-expected ratio was applied for (1) all heatwaves days that have occurred within the SPS and reached all the state mesoregions simultaneously, filtered for September and October, and (2) all fire-count spike days, when daily fire counts in the SPS surpassed the 90th percentile of the 2012–2019 period (277 fire counts), filtered for September and October. We also included an analysis of the lag effects in the mortality for fire-count spike days, considering 1, 2, and 3 days after the fire spike.

Atmospheric chemistry and transport modeling

The HYSPLIT atmospheric dispersion model from NOAA's Air Resources Laboratory was used to track wildfire smoke using forward and backward trajectory simulations⁹⁷. Meteorological data for the 3D trajectories were obtained from the NCEP Global Forecast System (GFS) dataset (<http://www.ready.noaa.gov/archives.php>), which provides $0.25^\circ \times 0.25^\circ$ spatial resolution, 55 vertical levels, and a 3-h temporal resolution. Simulation of 48-h forward trajectories at 1500 m above ground level (a.g.l.) from the Brazilian Pantanal (17.72°S , 56.03°W) and 48-h backward trajectories from São Paulo (23.51°S , 46.70°W) at 1800 UTC facilitated understanding of pollutant transport over different spatial and temporal scales. This approach allows for the visualization of airflow patterns and facilitates understanding pollutant transport over multiple spatial and temporal scales.

Moreover, the European Air Pollution Dispersion–Inverse Model (EURAD-IM) was used for mesoscale atmospheric chemistry and transport modeling^{98,99}. It utilizes the Weather Research and Forecast (WRF) model¹⁰⁰ as an offline meteorological model driver. The meteorological initial and boundary conditions are sourced from the United States National Center for Environmental Prediction (NCEP) Global Forecast System (GFS) at a horizontal resolution of $0.25^\circ \times 0.25^\circ$ (available at <https://rda.ucar.edu/datasets/ds083.3/>). The EDGAR v4.3.2 anthropogenic emission inventory¹⁰¹ is applied within the model domain for simulations. EURAD-IM employs data from the global Copernicus Atmosphere Monitoring Service (CAMS) Integrated Forecasting System (IFS) model as chemical initial and boundary conditions. Fire emissions are sourced from the Global Fire Assimilation System Version 1.2 (GFASv1.2) products, with a horizontal resolution of $0.1^\circ \times 0.1^\circ$ (available at <http://apps.ecmwf.int/datasets/data/cams-gfas>). The off-line model encompasses the south of Latina America focused on São Paulo with a 25 km horizontal resolution grid with 110×101 points covering an area of $2750 \times 2525 \text{ km}^2$, including crucial regions in southern and southeastern Brazil adjacent to São Paulo. Other model configurations and parameterizations are detailed in Table S3. Four EURAD-IM simulations were conducted to evaluate biomass-burning contributions during the P20F. The first simulation (NO_GFAS) excluded GFAS fire emissions. The second (GFAS_SP) included GFAS fire emissions over São Paulo State, Rio de Janeiro State, and part of Minas Gerais. The third (GFAS_PANT) focused exclusively on GFAS fire emissions over the Pantanal region. Finally, the fourth EURAD-IM simulation (GFAS_BR) was performed with GFAS fire emissions over the entire model domain.

Data availability

The data underlying the results presented in the study are available from Satellite-derived burned area data provided by the ALerta de Área queimada com Monitoramento Estimado por Satélite (ALARMES, <https://alarmes.lasa.ufrj.br>). Daily information on active fire counts over the SPS was obtained from NASA/NOAA's Visible Infrared Imaging Radiometer Suite (VIIRS, <https://firms.modaps.eosdis.nasa.gov>). Temperature and total precipitation data were obtained from the ECMWF reanalysis version 5 (ERA5) dataset (<https://www.ecmwf.int/en/forecasts/dataset/ecmwf-reanalysis-v5>). PM_{2.5} data were provided by the São Paulo State Environmental Company (CETESB, <https://cetesb.sp.gov.br/ar/qualar>). Daily mortality data from the Brazilian Health Informatics Department (DATASUS) were provided by the Data Science Platform applied to Health (PCDaS) of the Oswaldo Cruz Foundation (<https://pcdas.icict.fiocruz.br>). HYSPLIT meteorological input files are publicly available and archived on the NOAA ARL FTP site (<https://www.ready.noaa.gov/archives.php>). Meteorological initial and boundary conditions and fire emissions used for mesoscale atmospheric chemistry and transport modeling with the European Air Pollution Dispersion–Inverse Model (EURAD-IM) were provided by the United States National Center for Environmental Prediction (NCEP) Global Forecast System (GFS) (available at <https://rda.ucar.edu/datasets/ds083.3/>) and from the Global Fire Assimilation System Version 1.2 (GFASv1.2) products (available at <http://apps.ecmwf.int/datasets/data/cams-gfas>). Availability of model data: The authors will provide model data upon request.

Code availability

The authors will provide any code upon request.

Received: 26 March 2024; Accepted: 21 October 2024;

Published online: 08 November 2024

References

- Eyring, V. et al. Reflections and projections on a decade of climate science. *Nat. Clim. Chang.* **11**, 279–285 (2021).
- Sutanto, S. J., Vitolo, C., Di Napoli, C., D'Andrea, M. & Van Lanen, H. A. J. Heatwaves, droughts, and fires: Exploring compound and cascading dry hazards at the pan-European scale. *Environ. Int.* **134**, 105276 (2020).
- de Ruiter, M. C. et al. Why we can no longer ignore consecutive disasters. *Earths Future* **8**, e2019EF001425 (2020).
- Zhang, S. et al. Increased human risk caused by cascading hazards—A framework. *Sci. Total Environ.* **857**, 159308 (2023).
- Abatzoglou, J. T. & Williams, A. P. Impact of anthropogenic climate change on wildfire across western US forests. *Proc. Natl. Acad. Sci. USA* **113**, 11770–11775 (2016).
- Burke, M. et al. The contribution of wildfire to PM_{2.5} trends in the USA. *Nature* **622**, 761–766 (2023).
- Vara-Vela, A. L. et al. A new predictive framework for amazon forest fire smoke dispersion over South America. *Bull. Am. Meteorol. Soc.* **102**, E1700–E1713 (2021).
- Holanda, B. A. et al. African biomass burning affects aerosol cycling over the Amazon. *Commun. Earth Environ.* **4**, 1–15 (2023).
- Kemter, M. et al. Cascading hazards in the aftermath of Australia's 2019/2020 black summer wildfires. *Earths Future* **9**, e2020EF001884 (2021).
- Swain, D. L., Langenbrunner, B., Neelin, J. D. & Hall, A. Increasing precipitation volatility in twenty-first-century California. *Nat. Clim. Chang.* **8**, 427–433 (2018).
- Osman, M., Zaitchik, B. F. & Winstead, N. S. Cascading drought-heat dynamics during the 2021 southwest united states heatwave. *Geophys. Res. Lett.* **49**, e2022GL099265 (2022).
- Christian, J. I., Basara, J. B., Hunt, E. D., Otkin, J. A. & Xiao, X. Flash drought development and cascading impacts associated with the 2010 Russian heatwave. *Environ. Res. Lett.* **15**, 094078 (2020).

13. Zscheischler, J. et al. Future climate risk from compound events. *Nat. Clim. Chang.* **8**, 469–477 (2018).
14. Shaposhnikov, D. et al. Mortality related to air pollution with the moscow heat wave and wildfire of 2010. *Epidemiology* **25**, 359–364 (2014).
15. Salvador, C. et al. Effects of drought on mortality in macro urban areas of Brazil Between 2000 and 2019. *GeoHealth* **6**, e2021GH000534 (2022).
16. Santos et al. Twenty-first-century demographic and social inequalities of heat-related deaths in Brazilian urban areas. *PLoS ONE* **19**, e0295766 (2024).
17. Vicedo-Cabrera, A. M. et al. The burden of heat-related mortality attributable to recent human-induced climate change. *Nat. Clim. Chang.* **11**, 495–500 (2021).
18. Machado-Silva, F. et al. Drought and fires influence the respiratory diseases hospitalizations in the Amazon. *Ecol. Indic.* **109**, 105817 (2020).
19. Madaniyazi, L. et al. Seasonality of mortality under climate change: a multicountry projection study. *Lancet Planet. Health* **8**, e86–e94 (2024).
20. Niggli, L., Huggel, C., Muccione, V., Neukom, R. & Salzmann, N. Towards improved understanding of cascading and interconnected risks from concurrent weather extremes: Analysis of historical heat and drought extreme events. *PLoS Clim.* **1**, e0000057 (2022).
21. Libonati, R. et al. Assessing the role of compound drought and heatwave events on unprecedented 2020 wildfires in the Pantanal. *Environ. Res. Lett.* **17**, 015005 (2022).
22. Raymond, C. et al. Increasing spatiotemporal proximity of heat and precipitation extremes in a warming world quantified by a large model ensemble. *Environ. Res. Lett.* **17**, 035005 (2022).
23. Mukherjee, S. & Mishra, A. K. Increase in Compound Drought and Heatwaves in a Warming World. *Geophys. Res. Lett.* **48**, e2020GL090617 (2021).
24. Tripathy, K. P., Mukherjee, S., Mishra, A. K., Mann, M. E. & Williams, A. P. Climate change will accelerate the high-end risk of compound drought and heatwave events. *Proc. Natl. Acad. Sci. USA* **120**, e2219825120 (2023).
25. Geirinhas, J. L. et al. Combined large-scale tropical and subtropical forcing on the severe 2019–2022 drought in South America. *NPJ Clim. Atmos. Sci.* **6**, 1–13 (2023).
26. Libonati, R. et al. Drought–heatwave nexus in Brazil and related impacts on health and fires: A comprehensive review. *Ann. N. Y. Acad. Sci.* **1517**, 44–62 (2022).
27. Libonati, R., DaCamara, C. C., Peres, L. F., Sander De Carvalho, L. A. & Garcia, L. C. Rescue Brazil’s burning Pantanal wetlands. *Nature* **588**, 217–219 (2020).
28. Garcia, L. C. et al. Record-breaking wildfires in the world’s largest continuous tropical wetland: integrative fire management is urgently needed for both biodiversity and humans. *J. Environ. Manage.* **293**, 112870 (2021).
29. Tomas, W. M. et al. Distance sampling surveys reveal 17 million vertebrates directly killed by the 2020’s wildfires in the Pantanal, Brazil. *Sci. Rep.* **11**, 23547, <https://doi.org/10.1038/s41598-021-02844-5> (2021).
30. dos Santos Ferreira, B. H. et al. Wildfires Jeopardise Habitats of Hyacinth Macaw (*Anodorhynchus hyacinthinus*), a flagship species for the conservation of the Brazilian Pantanal. *Wetlands* **43**, 47 (2023).
31. Kumar, S. et al. Changes in land use enhance the sensitivity of tropical ecosystems to fire–climate extremes. *Sci. Rep.* **12**, 964 (2022).
32. Martins, P. I., Belém, L. B. C., Szabo, J. K., Libonati, R. & Garcia, L. C. Prioritising areas for wildfire prevention and post-fire restoration in the Brazilian Pantanal. *Ecol. Eng.* **176**, 106517 (2022).
33. Lorenz, C. et al. Wildfire and smoke association with COVID-19 cases in the Pantanal wetland, Brazil. *Public Health* **225**, 311–319 (2023).
34. Lorenz, C. et al. Could the compound effects of drought and fire have caused an increase of COVID-19 cases in the Pantanal wetland? *Wetl. Ecol. Manag.* **32**, 133–137 (2024).
35. Marengo, J. A. et al. Extreme drought in the Brazilian Pantanal in 2019–2020: characterization, causes, and impacts. *Front. Water* **3**, 639204 (2021).
36. Thielen, D. et al. The Pantanal under Siege—on the origin, dynamics and forecast of the megadrought severely affecting the largest wetland in the world. *Water* **13**, 3034 (2021).
37. Shi, L., Ding, R., Hu, S., Li, X. & Li, J. Extratropical impacts on the 2020–2023 Triple-Dip La Niña event. *Atmos. Res.* **294**, 106937 (2023).
38. Fasullo, J. T., Rosenbloom, N. & Buchholz, R. A multiyear tropical Pacific cooling response to recent Australian wildfires in CESM2. *Sci. Adv.* **9**, eadg1213 (2023).
39. Marengo, J. A. et al. The heat wave of October 2020 in central South America. *Int. J. Climatol.* **42**, 2281–2298 (2022).
40. Calim Costa, M., Marengo, J. A., Alves, L. M. & Cunha, A. P. Multiscale analysis of drought, heatwaves, and compound events in the Brazilian Pantanal in 2019–2021. *Theor. Appl. Climatol.* **155**, 661–677 (2024).
41. Martins, L. D. et al. Long-range transport of aerosols from biomass burning over Southeastern South America and their implications on air quality. *Aerosol Air Qual. Res.* **18**, 1734–1745 (2018).
42. Orellana, J. D. Y., Marrero, L. & Horta, B. L. Excess deaths from respiratory causes in eight Brazilian metropolises during the first six months of the COVID-19 pandemic. *Cad. Saude Publica* **37**, e00328720 (2021).
43. Otero, N., Jurado, O. E., Butler, T. & Rust, H. W. The impact of atmospheric blocking on the compounding effect of ozone pollution and temperature: a copula-based approach. *Atmos. Chem. Phys.* **22**, 1905–1919 (2022).
44. Willers, S. M. et al. High resolution exposure modelling of heat and air pollution and the impact on mortality. *Environ. Int.* **89–90**, 102–109 (2016).
45. Ramos, A. M. et al. The compound event that triggered the destructive fires of October 2017 in Portugal. *iScience* **26**, 106141 (2023).
46. Rosário, N. Édo, Sena, E. T. & Yamasoe, M. A. South American 2020 regional smoke plume: intercomparison with previous years, impact on solar radiation, and the role of Pantanal biomass burning season. *Atmos. Chem. Phys.* **22**, 15021–15033 (2022).
47. Podlaha, A., Bowen, S., Lörinc, M., Kerschner, B. & Srivastava, G. *Weather, Climate & Catastrophe Insight: 2020 Annual Report*. 79 <https://www.aon.com/global-weather-catastrophe-natural-disasters-costs-climate-change-2020-annual-report/index.html> (2020).
48. Libonati, R. Megafires are here to stay — and blaming only climate change won’t help. *Nature* **627**, 10–10 (2024).
49. Santos, F. L. M. et al. Prescribed burning reduces large, high-intensity wildfires and emissions in the Brazilian Savanna. *Fire* **4**, 56 (2021).
50. de Andrade, A. S. R. et al. Implementation of fire policies in Brazil: an assessment of fire dynamics in Brazilian Savanna. *Sustainability* **13**, 11532 (2021).
51. Oliveira, M. R. et al. Indigenous brigades change the spatial patterns of wildfires, and the influence of climate on fire regimes. *J. Appl. Ecol.* **59**, 1279–1290 (2022).
52. de Miranda, R. M. et al. Urban air pollution: a representative survey of PM2.5 mass concentrations in six Brazilian cities. *Air Qual. Atmos. Health* **5**, 63–77 (2012).

53. Liu, J. et al. Framing sustainability in a telecoupled world. *Ecol. Soc.* **18**, 26 (2013).
54. Sikor, T. et al. Global land governance: from territory to flow? *Curr. Opin. Environ. Sustain.* **5**, 522–527 (2013).
55. de Arruda Moreira, G. et al. Influence of a biomass-burning event in PM2.5 concentration and air quality: a case study in the metropolitan area of São Paulo. *Sensors* **21**, 425 (2021).
56. Bencherif, H. et al. Investigating the long-range transport of aerosol plumes following the amazon fires (August 2019): a multi-instrumental approach from ground-based and satellite observations. *Remote Sens.* **12**, 3846 (2020).
57. Freitas, S. R. et al. Monitoring the transport of biomass burning emissions in South America. *Environ. Fluid Mech.* **5**, 135–167 (2005).
58. Hoelzemann, J. J. et al. Regional representativity of AERONET observation sites during the biomass burning season in South America determined by correlation studies with MODIS Aerosol Optical Depth. *J. Geophys. Res. Atmos.* **114**, D13301 (2009).
59. Andrade, M. et al. Air quality in the megacity of São Paulo: evolution over the last 30 years and future perspectives. *Atmos. Environ.* **159**, 66–82 (2017).
60. Shrivastava, M. et al. Recent advances in understanding secondary organic aerosol: Implications for global climate forcing. *Rev. Geophys.* **55**, 509–559 (2017).
61. Kumar, P. et al. New directions: from biofuels to wood stoves: the modern and ancient air quality challenges in the megacity of São Paulo. *Atmos. Environ.* **140**, 364–369 (2016).
62. Squizzato, R. et al. Beyond megacities: tracking air pollution from urban areas and biomass burning in Brazil. *NPJ Clim. Atmos. Sci.* **4**, 17 (2021).
63. Pereira, G. M. et al. Particulate pollutants in the Brazilian city of São Paulo: 1-year investigation for the chemical composition and source apportionment. *Atmos. Chem. Phys.* **17**, 11943–11969 (2017).
64. Ogura, A. P., Silva, A. Cda, Castro, G. B., Espindola, E. L. G. & Silva, A. Lda An overview of the sugarcane expansion in the state of São Paulo (Brazil) over the last two decades and its environmental impacts. *Sustain. Prod. Consum.* **32**, 66–75 (2022).
65. Paraiso, M. L., de, S. & Gouveia, N. Health risks due to pre-harvesting sugarcane burning in São Paulo State, Brazil. *Rev. Bras. Epidemiol.* **18**, 691–701 (2015).
66. França, D. et al. Pre-harvest sugarcane burning emission inventories based on remote sensing data in the state of São Paulo, Brazil. *Atmos. Environ.* **99**, 446–456 (2014).
67. Othman, M. et al. Spatial–temporal variability and health impact of particulate matter during a 2019–2020 biomass burning event in Southeast Asia. *Sci. Rep.* **12**, 7630 (2022).
68. Siddaway, J. M. & Petelina, S. V. Transport and evolution of the 2009 Australian Black Saturday bushfire smoke in the lower stratosphere observed by OSIRIS on Odin. *J. Geophys. Res. Atmos.* **116**, D06203 (2011).
69. Rogers, H. M., Ditto, J. C. & Gentner, D. R. Evidence for impacts on surface-level air quality in the northeastern US from long-distance transport of smoke from North American fires during the Long Island Sound Tropospheric Ozone Study (LISTOS) 2018. *Atmos. Chem. Phys.* **20**, 671–682 (2020).
70. Dos Santos, N. et al. Accumulation of trace element content in the lungs of Sao Paulo city residents and its correlation to lifetime exposure to air pollution. *Sci. Rep.* **12**, 11083 (2022).
71. Ye, T. et al. Short-term exposure to wildfire-related PM2.5 increases mortality risks and burdens in Brazil. *Nat. Commun.* **13**, 7651 (2022).
72. Requia, W. J., Amini, H., Mukherjee, R., Gold, D. R. & Schwartz, J. D. Health impacts of wildfire-related air pollution in Brazil: a nationwide study of more than 2 million hospital admissions between 2008 and 2018. *Nat. Commun.* **12**, 6555 (2021).
73. Wu, Y. et al. Wildfire-related PM2.5 and health economic loss of mortality in Brazil. *Environ. Int.* **174**, 107906 (2023).
74. Wen, B. et al. Ambient PM2.5 and productivity-adjusted life years lost in Brazil: a national population-based study. *J. Hazard. Mater.* **467**, 133676 (2024).
75. Sun, Y. et al. Global supply chains amplify economic costs of future extreme heat risk. *Nature* **627**, 797–804 (2024).
76. Lee, W. et al. Synergic effect between high temperature and air pollution on mortality in Northeast Asia. *Environ. Res.* **178**, 108735 (2019).
77. Vlaanderen, J. J. et al. The impact of ambient air pollution on the human blood metabolome. *Environ. Res.* **156**, 341–348 (2017).
78. Tilloy, A., Malamud, B. D., Winter, D. & Joly-Laugel, A. A review of quantification methodologies for multi-hazard interrelationships. *Earth Sci. Rev.* **196**, 102881 (2019).
79. Sousa, P. M. et al. Heat-related mortality amplified during the COVID-19 pandemic. *Int. J. Biometeorol.* **66**, 457–468 (2022).
80. Menezes, L. S. et al. Lightning patterns in the Pantanal: untangling natural and anthropogenic-induced wildfires. *Sci. Total Environ.* **820**, 153021 (2022).
81. Kharin, V. V. & Zwiers, F. W. Estimating extremes in transient climate change simulations. *J. Clim.* **18**, 1156–1173 (2005).
82. Zscheischler, J. & Seneviratne, S. I. Dependence of drivers affects risks associated with compound events. *Sci. Adv.* **3**, e1700263 (2017).
83. Junk, W. J. & da Cunha, C. N. Pasture clearing from invasive woody plants in the Pantanal: a tool for sustainable management or environmental destruction? *Wetl. Ecol. Manag.* **20**, 111–122 (2012).
84. Ivory, S. J., McGlue, M. M., Spera, S., Silva, A. & Bergier, I. Vegetation, rainfall, and pulsing hydrology in the Pantanal, the world’s largest tropical wetland. *Environ. Res. Lett.* **14**, 124017 (2019).
85. Correa, D. B., Alcântara, E., Libonati, R., Massi, K. G. & Park, E. Increased burned area in the Pantanal over the past two decades. *Sci. Total Environ.* **835**, 155386 (2022).
86. Pivello, V. R. et al. Understanding Brazil’s catastrophic fires: Causes, consequences and policy needed to prevent future tragedies. *Perspect. Ecol. Conserv.* **19**, 233–255 (2021).
87. Valente, F. & Laurini, M. Pre-harvest sugarcane burning: a statistical analysis of the environmental impacts of a regulatory change in the energy sector. *Clean. Eng. Technol.* **4**, 100255 (2021).
88. Pinto, M. M., Libonati, R., Trigo, R. M., Trigo, I. F. & DaCamara, C. C. A deep learning approach for mapping and dating burned areas using temporal sequences of satellite images. *ISPRS J. Photogramm. Remote Sens.* **160**, 260–274 (2020).
89. Schroeder, W., Oliva, P., Giglio, L. & Csaszar, I. A. The New VIIRS 375 m active fire detection data product: Algorithm description and initial assessment. *Remote Sens. Environ.* **143**, 85–96 (2014).
90. Hersbach, H. et al. ERA5 hourly data on single levels from 1940 to present. *Copernicus Climate Change Service (C3S) Climate Data Store (CDS)*. <https://doi.org/10.24381/cds.adbb2d47> (2023).
91. Nairn, J. R. & Fawcett, R. J. B. The excess heat factor: a metric for heatwave intensity and its use in classifying heatwave severity. *Int. J. Environ. Res. Public Health* **12**, 227–253 (2015).
92. Nairn, J., Ostendorf, B. & Bi, P. Performance of excess heat factor severity as a global heatwave health impact index. *Int. J. Environ. Res. Public Health* **15**, 2494 (2018).
93. Geirinhas, J. L. et al. Heat-related mortality at the beginning of the twenty-first century in Rio de Janeiro, Brazil. *Int. J. Biometeorol.* **64**, 1319–1332 (2020).
94. Vicente-Serrano, S. M. et al. A global drought monitoring system and dataset based on ERA5 reanalysis: A focus on crop-growing regions. *Geosci. Data J.* **10**, 505–158 (2022).
95. Liberato, M. L. R. et al. Rankings of extreme and widespread dry and wet events in the Iberian Peninsula between 1901 and 2016. *Earth Syst. Dyn.* **12**, 197–210 (2021).

96. Parente, J., Amraoui, M., Menezes, I. & Pereira, M. G. Drought in Portugal: current regime, comparison of indices and impacts on extreme wildfires. *Sci. Total Environ.* **685**, 150–173 (2019).
97. Draxler, R. R. & Hess, G. D. Description of the HYSPLIT_4 Modeling System. NOAA Technical Memorandum ERL ARL-224. <https://www.arl.noaa.gov/documents/reports/arl-224.pdf> (1997).
98. Memmesheimer, M. et al. Long-term simulations of particulate matter in Europe on different scales using sequential nesting of a regional model. *Int. J. Environ. Pollut.* **22**, 108–132 (2004).
99. Elbern, H., Strunk, A., Schmidt, H. & Talagrand, O. Emission rate and chemical state estimation by 4-dimensional variational inversion. *Atmos. Chem. Phys.* **7**, 3749–3769 (2007).
100. Skamarock, W. C. et al. A Description of the Advanced Research WRF Version 3. University Corporation for Atmospheric Research. <https://doi.org/10.5065/D68S4MVH> (2008).
101. Crippa, M. et al. Gridded emissions of air pollutants for the period 1970–2012 within EDGAR v4.3.2. *Earth Syst. Sci. Data* **10**, 1987–2013, <https://doi.org/10.5194/essd-2018-31> (2018).

Acknowledgements

We acknowledge the São Paulo State Environment Sanitation Technology Company (CETESB) for the PM_{2.5} data. We also would like to acknowledge the computing time granted through JARA on the supercomputer JURECA at Forschungszentrum Jülich (Jülich Supercomputing Center, 2018). The research behind it is a direct contribution to the research themes of Project Rede Pantanal (FINEP grant 01.20.0201.00) and the Klimapolis Laboratory (klimapolis.net). We acknowledge Beatriz Nunes for the design of Figure 7. We thank Anne Caroline Lange, Philipp Franke, and Elmar Friese of the Rhenish Institute for Environmental Research (RIU) and Research Centre Jülich (FZJ), Germany, for sharing the EURAD-IM model code and providing all needed support to adapt the model to the southern hemisphere. This work was developed under the scope of Project "[https://urldefense.com/v3/_http://OVERHEAT.SA_!!NLFgqXoFfo8MMQlvZAscTxqmOcCU0EKzKSYLUuBslFyWJBGLVcHS2CmmaL2HCyhd21H3QbVD6PSAnF8SZXHobbMI8AI5e2d8IduGTSSf6bklcDXDc\\$](https://urldefense.com/v3/_http://OVERHEAT.SA_!!NLFgqXoFfo8MMQlvZAscTxqmOcCU0EKzKSYLUuBslFyWJBGLVcHS2CmmaL2HCyhd21H3QbVD6PSAnF8SZXHobbMI8AI5e2d8IduGTSSf6bklcDXDc$)" OVERHEAT.SA - COLlaboratiVE Research on Compound Drought and HEATWave events in South America financed by CNPQ grant number 443285/2023-3. DMS was supported by FAPERJ [grant numbers 205.890/2022 and 205.891/2022]. A.M.O. acknowledges the support of Project Rede Pantanal (FINEP grant 01.20.0201.00). F.O.R. was supported by CNPq grant 302755/2018-7. R.L. was supported by CNPq [grant 311487/2021-1] and FAPERJ [grant E-26/200.329/2023]; J.A.R. was supported by Wetlands International Brasil/Mupan. L.S.M. was supported by the Coordenação de Aperfeiçoamento de Pessoal de Nível Superior - Brazil (CAPES) - Finance Code 001 [grant number 88887.839553/2023-00]; R.A. was supported by the Programa Institucional de Bolsa de Iniciação Científica - Universidade Federal do Rio de Janeiro (PIBIC-UFRJ); ESFD was supported by FCT - Fundação para a Ciência e Tecnologia, I.P., in the framework of the ICT project with the references UIDB/04683/2020 and UIDP/04683/2020 ("[https://doi.org/10.54499/UIDP/04683/2020](https://urldefense.com/v3/_https://doi.org/10.54499/UIDP/04683/2020_!!NLFgqXoFfo8MMQlvZAscTxqmOcCU0EKzKSYLUuBslFyWJBGLVcHS2CmmaL2HCyhd21H3QbVD6PSAnF8SZXHobbMI8AI5e2d8IduGTSSf6bpo8SMjg$)" and "[https://doi.org/10.54499/UIDB/04683/2020](https://urldefense.com/v3/_https://doi.org/10.54499/UIDB/04683/2020_!!NLFgqXoFfo8MMQlvZAscTxqmOcCU0EKzKSYLUuBslFyWJBGLVcHS2CmmaL2HCyhd21H3QbVD6PSAnF8SZXHobbMI8AI5e2d8IduGTSSf6btp5R-Dc$)"). ESFD, RL, LFP, and JJH acknowledge that their work has been carried out in the framework INCT Klimapolis, funded by CNPq, grant number 406728/2022-4). The funder played no role in the study design, data collection, data analysis and interpretation, or this manuscript's writing.

[https://doi.org/10.54499/UIDB/04683/2020_!!NLFgqXoFfo8MMQlvZAscTxqmOcCU0EKzKSYLUuBslFyWJBGLVcHS2CmmaL2HCyhd21H3QbVD6PSAnF8SZXHobbMI8AI5e2d8IduGTSSf6btp5R-Dc\\$](https://doi.org/10.54499/UIDB/04683/2020_!!NLFgqXoFfo8MMQlvZAscTxqmOcCU0EKzKSYLUuBslFyWJBGLVcHS2CmmaL2HCyhd21H3QbVD6PSAnF8SZXHobbMI8AI5e2d8IduGTSSf6btp5R-Dc$)" <https://doi.org/10.54499/UIDB/04683/2020>). ESFD, RL, LFP, and JJH acknowledge that their work has been carried out in the framework INCT Klimapolis, funded by CNPq, grant number 406728/2022-4). The funder played no role in the study design, data collection, data analysis and interpretation, or this manuscript's writing.

Author contributions

D.M.S.: Conceptualization, Methodology, Formal Analysis, Discussion, Writing & Final Review. A.M.O.: Methodology, Formal Analysis, Discussion & Writing. E.S.F.D.: Methodology, Formal Analysis, Discussion & Writing. J.A.R.: Formal Analysis, Discussion & Writing. L.S.M.: Formal Analysis, Discussion & Writing. R.A.: Formal Analysis, Discussion & Writing. F.O.R.: Discussion & Writing. L.F.P.: Discussion & Writing. J.J.H.: Conceptualization, Methodology, Supervision, Discussion, Writing & Final Review. R.L.: Funding Resources, Conceptualization, Methodology, Supervision, Discussion, Writing & Final Review.

Competing interests

The authors declare no competing interests.

Additional information

Supplementary information The online version contains supplementary material available at <https://doi.org/10.1038/s44304-024-00031-w>.

Correspondence and requests for materials should be addressed to Djacinto Monteiro dos Santos or Renata Libonati.

Reprints and permissions information is available at <http://www.nature.com/reprints>

Publisher's note Springer Nature remains neutral with regard to jurisdictional claims in published maps and institutional affiliations.

Open Access This article is licensed under a Creative Commons Attribution-NonCommercial-NoDerivatives 4.0 International License, which permits any non-commercial use, sharing, distribution and reproduction in any medium or format, as long as you give appropriate credit to the original author(s) and the source, provide a link to the Creative Commons licence, and indicate if you modified the licensed material. You do not have permission under this licence to share adapted material derived from this article or parts of it. The images or other third party material in this article are included in the article's Creative Commons licence, unless indicated otherwise in a credit line to the material. If material is not included in the article's Creative Commons licence and your intended use is not permitted by statutory regulation or exceeds the permitted use, you will need to obtain permission directly from the copyright holder. To view a copy of this licence, visit <http://creativecommons.org/licenses/by-nc-nd/4.0/>.

© The Author(s) 2024, corrected publication 2024